PAPER

Characterization of Ce:CSSO, Pr:CSSO, and co-doped Ce,Pr:CSSO phosphors for aerosol phosphor thermometry

To cite this article: Joshua M Herzog *et al* 2021 *Meas. Sci. Technol.* **32** 054008

Characterization of Ce:CSSO, Pr:CSSO, and co-doped Ce,Pr:CSSO phosphors for aerosol phosphor thermometry

Joshua M. Herzog, Dustin Witkowski, David A. Rothamer

University of Wisconsin–Madison, Department of Mechanical Engineering, 1500 Engineering Dr., Madison, WI 53706, USA

E-mail: jherzog2@wisc.edu

November 2020

Abstract. The phosphor Ce:$Ca_3Sc_2Si_3O_{12}$(Ce:CSSO) was recently investigated for aerosol phosphor thermometry (APT) and shown to be capable of temperature imaging up to at least 1400 K. To date, no thorough characterization of the temperature dependent emission properties of the phosphor has been performed up to 1400 K. Additionally, due to limited sensitivity over certain temperature ranges continuous temperature imaging from 300 to 1400 K was not possible. Here, cerium and praseodymium doped into CSSO are investigated to address these limitations. Singly-doped Ce:CSSO and Pr:CSSO, and co-doped Ce,Pr:CSSO phosphor samples were studied. Emission lifetimes and quenching behavior were characterized in a tube furnace for each phosphor. Results from the singly-doped phosphors were used to interpret the co-doped phosphor results. The phosphor characterization data was used to estimate thermometry performance at temperatures relevant to low-temperature ignition studies in engines. The proposed diagnostic uses a combination of co-doped APT, host-referenced APT, and scattering-referenced APT (SRAPT) approaches to increase the range over which high-precision temperature measurements can be made. Characterization results include the first reported measurements of luminescence lifetimes for Ce:CSSO and Pr:CSSO at temperatures up to 1400 K, and the highest reported quenching temperature for a phosphor using $4f5d$ emission (1230 K for Ce:CSSO). Furnace measurements showed a normalized temperature-sensitivity of $> 0.25\%$/K from room temperature to 1400 K for at least one diagnostic approach using the co-doped Ce,Pr:CSSO phosphor. Estimates suggest that the co-doped Ce,Pr:CSSO phosphor is feasible for APT at temperatures ranging from 300 to 925 K and 1030 to at least 1400 K, with better than 40-K single-shot precision. The performance of Ce:CSSO and Ce,Pr:CSSO are similar throughout the investigated temperature range.

Keywords: thermometry, phosphor, co-doped, CSSO, thermal quenching

Submitted to: *Meas. Sci. Technol.*

1. Introduction

Aerosol phosphor thermometry (APT) is a temperature imaging technique that relies on temperature-dependent, laser-excited luminescence emission from small particles seeded into a flow [1]. Although APT appears to be a promising tool for combustion studies, several significant limitations still exist. In particular, phosphor's that exhibit fast, bright emission with high temperature-sensitivity required for precise temperature measurements above 1000 K are currently lacking in the literature.

Recently, Ce^{3+} doped into calcium scandium silicate ($Ca_3Sc_2Si_3O_{12}$; CSSO), was demonstrated to be capable of aerosol phosphor thermometry measurements at temperatures of at least 1400 K [2] using a scattering-referenced approach. This measurement represented a significant increase in the maximum temperature measured using APT, which previously had been limited to less than 1000 K [3], and demonstrated the potential for APT in combustion-relevant flows. Although the previous Ce:CSSO measurements were successful in increasing the maximum temperature measurable with APT, there were a few drawbacks to the method. Namely, Ce^{3+} emission intensity is not strongly temperature-sensitive at temperatures less than 1000 K, limiting the range of measured temperatures. In [2], host defect emission was used in combination with Ce^{3+} emission in a host-referenced APT approach to provide temperature measurements between 600-800 K, but this was still not sufficient to provide a continuous temperature measurement throughout the entire 300-1400 K range. Additionally, no detailed characterization of the Ce:CSSO phosphor for thermometry was available to aid in experiment design, although previous measurements indicated there is no significant thermal quenching until at least 860 K [4].

In the remainder of this paper, we characterize the Ce:CSSO, Pr:CSSO, and Ce,Pr:CSSO phosphors to address these limitations. Co-doping with Pr^{3+} is proposed to provide an alternative low-quenching-temperature emission band that can be used for temperature imaging until the onset of thermal quenching in the Ce^{3+} emission band. Measurements of luminescence lifetime in Pr:CSSO have shown significant quenching occurring near 600-700 K [5], with emission intensity peaking at wavelengths near 320 and 370 nm (significantly blue-shifted from the Ce^{3+} emission peak), making Pr^{3+} an attractive co-dopant for temperature measurements below 1000 K. Singly-doped Ce:CSSO and Pr:CSSO are suitable phosphors for APT measurements over moderate temperature ranges by themselves and, as such, the more complete characterization of these phosphors for APT provided here is merited. Additionally, characterization of the singly-doped phosphors is needed to aid in the interpretation of the co-doped phosphor data.

Phosphor characterization was performed in a temperature-controlled tube furnace at temperatures up to 1400 K. Luminescence decay curves and emission spectra were recorded at 100 K intervals to measure emission intensity, spectral bandshapes, and luminescence lifetimes as a function of temperature. Lifetime data is used to analyze thermal quenching for each phosphor and ion, and the spectral data and lifetime data are used in combination to estimate relative emission intensities as a function of temperature. The relative emission intensities are used to calculate the temperature sensitivity for a variety of APT techniques including scattering-referenced APT (SRAPT), co-doped APT, and host-referenced APT. Finally, performance estimates for an ideal experimental setup are made to compare each of the different phosphor compositions and APT techniques.

2. Background

For each of the APT approaches discussed here (including co-doped APT [6], host-referenced APT [7], and SRAPT [8]), temperature is determined through measurement of a signal ratio. The measured ratio of signals can be written as

$$R = \frac{S_2}{S_1} \tag{1}$$

where S_i is the measured intensity (in counts) in band i. For SRAPT, S_2 is the (assumed constant) scattering intensity while for co-doped and host-referenced APT, S_1 and S_2 are both emission bands. Temperature dependence of the ratio for the two techniques arises because one of the signals is relatively constant with temperature, while the other is changing rapidly due to thermal quenching. We have adopted the convention of having the numerator (S_2) be the relatively temperature independent reference signal, and the denominator (S_1) be the signal whose thermal quenching provides the majority of the temperature sensitivity. Therefore, the ratio increases rapidly with temperature once thermal quenching of S_1 becomes significant.

In the case of co-doped APT, the two signals originate from luminescence emission from the two ions doped into the same host material. Specifically for Ce,Pr:CSSO, S_1 is the $4f5d$ emission from Pr^{3+}, whereas, S_2 is the $4f5d$ emission from Ce^{3+}. The emission from Pr^{3+} quenches at a lower temperature than that for Ce^{3+} in CSSO; therefore, Ce^{3+} serves as the reference signal in this instance, although both signals are temperature dependent. For SRAPT

measurements, elastic light scattering (Mie scattering) from the seeded phosphor particles provides the reference signal (S_2) and the luminescence signal from a single ion (either Ce^{3+} or Pr^{3+}) is used as the highly temperature dependent signal S_1. For host-referenced APT with the Ce:CSSO phosphor, S_1 is taken as the host emission as it quenches at lower temperatures than Ce^{3+}.

The normalized temperature sensitivity of a ratiometric temperature measurement technique is defined as

$$\xi_T = \frac{1}{R}\frac{\partial R}{\partial T} = \frac{1}{S_2}\frac{\partial S_2}{\partial T} - \frac{1}{S_1}\frac{\partial S_1}{\partial T} \tag{2}$$

and the temperature precision s_T (estimated temperature standard deviation) is calculated by first order uncertainty propagation as [1]

$$s_T = \frac{s_R}{\xi_T\, R} \tag{3}$$

where s_R is the ratio measurement precision index (estimated ratio standard-deviation). The quantity R/s_R is the signal-to-noise ratio for the intensity ratio measurement, and is related to the signal measurement precision index, s_{S_i} for band i. It should be noted that the techniques work even if S_2 has some temperature dependence; if S_2 is increasing with temperature as S_1 decreases, then the sensitivity is actually improved; similarly, sensitivity is decreased if S_2 decreases with temperature.

Luminescence intensity, and hence intensity ratios, changes primarily as a result of thermal quenching and is strongly dependent on the characteristic energy gap for the quenching process [9]. For typical inorganic phosphors doped with rare-earth ions, thermal quenching can result from both nonradiative deactivation to the vibrationally excited ground-state and ionization to the conduction band [10]. However, in many cases the quenching can be explained by a single dominant mechanism which can be identified through an electronic structure diagram [11]. A vacuum-referred binding energy (VRBE) electronic structure diagram with harmonic potential energy curves superimposed was calculated according to the theory of Dorenbos [12]. Parameters for the CSSO host (specifically U, E^{ex}, D, E^{CT}, and $E_{Eu^{2+};4f}$ of the chemical shift model) are taken from [4], and a harmonic oscillator stiffness ratio ($k_{5d}/k_{4f} = 0.7$) was chosen to approximately match the quenching behavior observed here. The harmonic oscillator stiffness ratio is based on previous work analyzing quenching behavior of Ce^{3+} and Pr^{3+} in garnet hosts [11].

The VRBE diagram for Ce^{3+} and Pr^{3+} doped into CSSO is presented in Figure 1. From the diagram, the primary quenching mechanism for Ce^{3+} appears to be ionization to the conduction band with an energy gap ≈ 1.4 eV, whereas Pr^{3+} quenches primarily

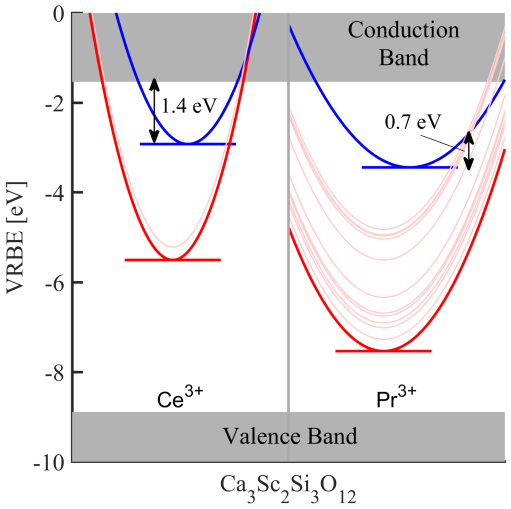

Figure 1: Calculated vacuum-referred binding energy diagram for Ce^{3+} and Pr^{3+} in CSSO with harmonic potential energy curves superimposed. The red curves indicate the ground $4f$ states, pink curves indicate higher $4f$ states, and blue curves indicate the $5d$ states.

via nonradiative deactivation to a $4f$ state with an energy gap closer to 0.7 eV. Thermal ionization rates follow an Arrhenius dependence [13], such that the 50%-quenching temperature (T_{50}, the temperature at which the luminescence quantum yield is reduced by a factor of 2) is directly proportional to the smallest characteristic energy gap, or

$$T_{50} = \frac{E_i}{k_B} \frac{1}{\ln\left(C_{NR}/A_R\right)}, \tag{4}$$

where E_i is the energy gap, k_B is the Boltzmann constant, C_{NR} is the non-radiative attempt rate, and A_R is the radiative deactivation rate.

The large difference in energy gap is indicative of the quenching characteristics of the two ions; Ce^{3+} is expected to quench at much higher temperature than Pr^{3+}. From this diagram, T_{50} for Ce^{3+} is approximately 1000 K, assuming a radiative decay rate of 20 MHz[1] and a non-radiative attempt rate of 30 THz (see [14] for a detailed discussion of thermal quenching as it relates to the VRBE diagram; from [14], the non-radiative attempt rate is similar to the maximum phonon frequency of the host, which is typically on the order of 30 THz). In contrast, T_{50} for Pr^{3+} is around 600 K (assuming a radiative decay rate of 50 MHz[2], and the same attempt rate as Ce^{3+}).

It is worth noting that with 266-nm (4.66 eV) excitation Ce^{3+} 4f electrons are promoted to the conduction band; this may be partly responsible for the observed host emission. Exciting Pr^{3+} at 266 nm

[1] This corresponds to a ~50 ns room-temperature lifetime
[2] This corresponds to a ~20 ns room-temperature lifetime

does not promote electrons to the conduction band and, as will be seen in the results, no host emission is observed for the singly-doped Pr:CSSO phosphor. Exciting at wavelengths shorter than ∼220 nm (5.64 eV), corresponding to the energy gap between the Pr^{3+} $4f$ level and the conduction band minimum, has been shown to result in host emission in Pr:CSSO [5] similar to that observed in Ce:CSSO and Ce,Pr:CSSO for 266-nm excitation.

3. Experimental Methods and Materials

Three phosphor samples were characterized: Ce:CSSO, Pr:CSSO, and Ce,Pr:CSSO, each at a doping level of 0.5% per ion. Phosphor samples were manufactured by Phosphor Technology Ltd., with specifications summarized in Table 1. The mass density of the phosphor materials is assumed to be equal to that of the host, which is approximately 3510 kg/m^3 [15]. Heat capacity is assumed to be the same for each sample as well, and was measured and presented in [2], where the Debye temperature was found to be 878 K and the Dulong-Petit heat capacity is 1020 J/kg-K; these values will be used later to quantify intrusiveness for performance estimates.

As noted in [2], Ce:CSSO exhibits a significant amount of host defect emission when excited at 266 nm. To reduce interference and better observe the photophysical properties of the rare-earth ions, the Ce:CSSO and Ce,Pr:CSSO phosphor samples were annealed. The annealing process involved heating the phosphor to 1400 K in a furnace, holding for 10 minutes, then cooling to room temperature with a ramp rate of 300 K/hour (for both heating and cooling); annealing was found to reduce the host emission significantly, but did not eliminate it. Subsequent heating and cooling of annealed phosphor samples resulted in almost no change in emission characteristics. Data and analysis are presented for the annealed Ce:CSSO and Ce,Pr:CSSO samples only to enable repeatable measurements; since data were taken in a furnace annealing would occur during the process of data acquisition if not done ahead of time. For Pr:CSSO no significant change in luminescence properties was observed due to prolonged heating (*i.e.*, annealing) and no annealing of the samples was done prior to data acquisition.

Characterization of the phosphor samples was performed in a tube furnace (CM Furnaces, Rapid Temp Model 1720-12). A schematic of the experimental setup is shown in Figure 2. Phosphor samples were placed in a small aluminum oxide (a refractory material suitable for high-temperature studies) dish inside the furnace and were excited with the 266-nm 4$^{\text{th}}$-harmonic output of a flashlamp-pumped Nd:YAG laser (Ekspla, NL-303D-10-SH/TH/FH) operated at 10 Hz, with a pulse energy of 0.5±0.1 mJ/pulse (fluence = 1.3 ± 0.3 mJ/cm^2; this uncertainty corresponds to shot-to-shot variation) after passing through a variable attenuator. The laser pulse width is approximately 6 ns FWHM based on manufacturer specifications.

Emission spectra were measured using a spectrometer (Acton SP-2300i; 300 groove/mm, 500-nm blazed grating) with an intensified charge-coupled device (ICCD) camera (Princeton Instruments, PI-MAX4 1024i-HB-FG-18-P46) resulting in a measured spectral resolution of 2-nm FWHM. Light was captured using a 25-mm diameter UV-grade fused silica lens with 500-mm focal length. Light was focused onto the end of an optical fiber bundle that was connected to the entrance slit of the spectrometer. The spectrometer was outfitted with a long-pass filter (Schott WG-295, 3mm) to reject scattered laser light. For each sample, a series of 200 single-shot spectra are acquired and averaged.

Time-resolved luminescence was measured using a photomultiplier tube (PMT) module (Hamamatsu, H5783), with a rise time of 0.78 ns (based on manufacturer specifications). Ce^{3+} emission was collected in a wavelength band from 500 to 575 nm using a combination of interference and colored glass filters (500-nm longpass filter, Corion LL-500-S[3]; 575-nm shortpass filter, Reynard R00925-00; and a UV-rejection filter, Schott WG-295 6 mm). Host and Pr^{3+} emission was captured in a wavelength band from 295 to 425 nm using a different set of filters (425-nm shortpass filter, Edmund Optics 84-716; and a UV-rejection filter, Schott WG-295 6 mm), which is referred to throughout as the host-Pr^{3+} emission band. In both cases, an additional 532-nm notch filter (Semrock Inc., NF01-532U) was used to reject any residual 532-nm laser light in the room. Filter bands were chosen to avoid interference from $4f$ emission. The PMT module was outfitted with a 105-mm $f/2.8$ lens (Nikon, Micro-Nikkor), and the lens f-number was varied to approximately match emission intensity recorded by the PMT. The PMT was setup to operate linearly, avoiding saturation, such that photocurrent is proportional to collection efficiency. The time-resolved results were averaged over 256 single-shot samples to reduce noise.

3.1. Lifetime fitting

Luminescence lifetimes were calculated using a multiple-exponential fitting algorithm applied to the decay curves starting 3 ns after the peak measured intensity. Rise times (5% to 100% of the peak) were larger than 4 ns for all samples; 3 ns after the peak is

[3] No spectrally-resolved transmission was available for this filter; the filter is instead modeled as a perfect long-pass filter with 500 nm cut-off wavelength and 90% transmission.

Table 1: Phosphor specifications for each composition as reported by the manufacturer Phosphor Technology Ltd. $\bar{d}$ is the manufacturer-reported volume-weighted median particle diameter.

Phosphor	Part #	Doping [%]	$\bar{d}$ [µm]
Ce:CSSO	FNBK58/FF-X	0.5	1.4
Pr:CSSO	FNBK59/FF-X	0.5	1.5
Ce,Pr:CSSO	FNBK58P/FF-X	0.5 ea.	1.5

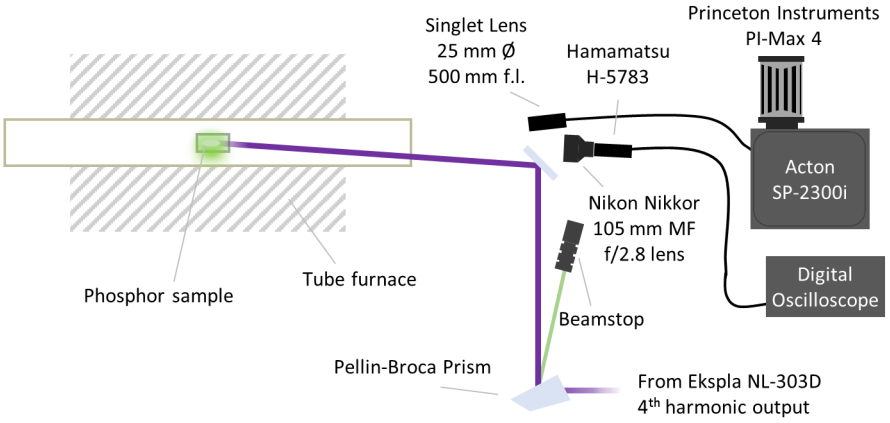

Figure 2: Experimental setup diagram for phosphor characterization experiments.

sufficient that the fitting procedure is not significantly impacted by the laser. The last 100 data points (approximately 25 ns) are averaged and subtracted from the data series before fitting; this is recommended by [16] to ensure integrals of the decay curves are bounded and should have no impact on the fit results. The curve-fitting procedure is outlined in the following paragraphs.

The first step of the fitting procedure applies the Pade-Laplace-AIC (PLA) algorithm (as described in [16]) to estimate the number of exponential terms in the decay curves, and the corresponding lifetimes for each component. This procedure finds both real and complex roots; however, for our purposes, only solutions with real roots were kept. The PLA procedure makes use of the Akaike Information Criterion (AIC) [17] to determine the correct number of terms without overfitting the data.

The PLA procedure provides a good initial guess for the exponential parameters, but is not optimized in the least squares sense. To remedy this, a non-linear least squares (NLLS) method was implemented as the second step in the algorithm. The NLLS method uses the variable projection method as described in [18]. The NLLS fit is repeated with a variable sized fitting window based on the shortest and longest lifetimes (such that $t \in [k_1\tau_{min,i}, k_2\tau_{max,i}]$ where k_1 and k_2 are constants; here $k_1 = 0.25$ and $k_2 = 5.0$) until the best-fit parameters converge (sum of normalized squared error $< 10^{-5}$). In general, convergence occurred within two iterations, but several data sets required additional iterations, particularly when significant noise or non-exponential behavior was present in the data. The iterative procedure is based on the single-exponential fitting procedure developed and reported in [19], but here is adapted to allow for fitting of multiple exponentials. The NLLS method was weighted assuming the measurements are shot-noise limited; sample variance is assumed to be proportional to intensity.

For much of the data shown here, two or three exponentials were needed to adequately fit the data. For multi-exponential decays, the signal-weighted average lifetime is reported as [20]

$$\bar{\tau} = \frac{\sum c_i \tau_i^2}{\sum c_i \tau_i}, \tag{5}$$

where the c_i is the intensity of the ith exponential component.

Sample data and fit results are shown for both the Ce^{3+} and Pr^{3+} emission bands of Ce,Pr:CSSO in Figure 3. For the room temperature results shown, Pr^{3+} was fit with a double exponential with lifetimes of ∼30 ns (corresponding to $4f5d$ emission) and ∼5 ns. The source of the fast component is not clear, but it may be related to observed host emission that will be discussed in Section 4.1. For Ce^{3+}, three terms

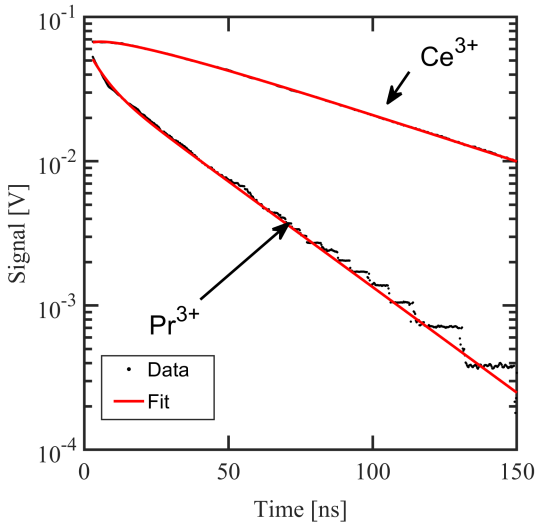

Figure 3: Luminescence decay curves and curve fits of the Ce,Pr:CSSO phosphor at room temperature for Ce^{3+} and Pr^{3+}.

were needed with lifetimes of 67 ns (corresponding to $4f5d$ emission), 20 ns and 5 ns. The shorter lifetime components for Ce^{3+} appear to correspond to feeding of the Ce^{3+} $5d$ level. The weighted average lifetimes are 70 and 27 ns for Ce^{3+} and Pr^{3+}, respectively.

From the plot, the early time behavior is well-represented by the fit but at later times there is more significant deviation, particularly in the case of the Pr^{3+} band. The PLA algorithm tends to underestimate the complexity of the data [16] (typically reporting a lower bound on the number of exponential terms present in the data); it is therefore likely that some of the observed discrepancy at late times is due to the presence of a longer lifetime (or constant offset) component in the data that was not fit. However, since the disagreement is small compared to the peak observed signal levels, the fit is believed to be sufficient to describe the $4f5d$ and host defect components of the emission that are of interest for thermometry.

3.2. Emission intensity

The temperature dependence of the emission intensity for each ion is calculated by integrating the emission spectrum over wavelength, and normalizing the result to unity at room temperature; the emission spectra integrated over their respective filter bands are used to determine the temperature-dependence of the total signal intensity. The relative room temperature signal of each ion or band was determined from the integrated luminescence decay data at room temperature, scaled to account for differences in laser energy, lens aperture, optical efficiencies, and PMT photocathode quantum efficiency. Optical and quantum efficiencies are corrected based on manufacturer supplied data and are thus only approximate. Since no transmission data was available for the Nikon 105 mm lens, lens transmission is assumed to be identical to that of the Nikon 135 mm lens reported by [21].

As investigated in [22], bulk powder measurements do not necessarily reflect changes in absorption cross-section, and the majority of the observed signal change in furnace measurements result largely from changes in luminescence quantum yield. More succinctly, furnace measurements may not be perfectly representative of aerosol particle emission intensity. We expect that the particle absorption cross-section does not change appreciably between the singly-doped and co-doped phosphors. Thus, the relative signal intensities are believed to be reflective of the relative differences in luminescence quantum yield that result from quenching and energy transfer processes occurring in the co-doped CSSO phosphor.

The aerosol performance estimates provided here are believed to be reasonably accurate despite the use of bulk powder data. As all of the phosphor materials tested here use the same host material and manufacturing method and have a similar particle size distribution, it is believed that the state of agglomeration and optical properties of the bulk powder samples did not change appreciably between the Pr:CSSO, Ce:CSSO and Ce,Pr:CSSO samples, and that the results are directly comparable. Further, all of the aerosol techniques under consideration rely primarily on thermal quenching, or changes in luminescence quantum efficiency. Performance estimates for these techniques are less prone to error (*e.g.*, due to preferential reabsorption) than spectral luminescence intensity ratio approaches.

4. Results and Discussion

4.1. Emission spectra

Normalized room temperature emission spectra comparing the co-doped and singly-doped phosphors are shown in Figure 4. There is a clear change in the emission band shape of Pr^{3+} following the introduction of Ce^{3+}. In particular, the peak centered near 370 nm is much brighter in the Ce,Pr:CSSO phosphor sample compared to Pr:CSSO. This is likely due to interfering host emission that is also present in Ce:CSSO. The Ce:CSSO phosphor emission has a clear Ce^{3+} emission band (450 nm to $>$ 600 nm) and a host emission peak (near 360 nm); the host emission peak clearly overlaps the Pr^{3+} emission, as is evident in the co-doped data. Interestingly, only a small portion (around 20%)

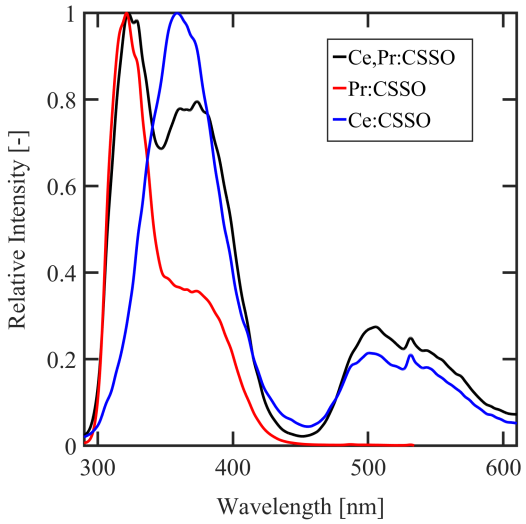

Figure 4: Normalized room-temperature emission spectra for co-doped Ce,Pr:CSSO (annealed) and singly doped Ce:CSSO (annealed) and Pr:CSSO.

of light emitted from the Ce:CSSO phosphor at room temperature, even after annealing, is associated with $4f5d$ emission; the remainder appears to be associated with host defects [5].

The temperature-dependent emission spectra of all three phosphors are shown in Figure 5. The singly-doped Pr:CSSO phosphor is shown in Figure 5a. The Pr:CSSO phosphor looks largely as expected, with two peaks centered near 320 and 370 nm. A small increase in emission intensity is observed at 400 K before the onset of thermal quenching. Peak emission intensity is reduced by more than a factor of 2 by 600 K. No host emission is apparent for 266-nm excitation; this is consistent with the results reported by [5], where host emission became significant when exciting at wavelengths $\leq$ 224 nm. The Pr:CSSO emission bandshape appears to be largely independent of temperature.

The Ce:CSSO sample, shown in Figure 5b, has a significant host-emission component peak near 360 nm. There is clear overlap between the $4f5d$ Ce^{3+} emission and the host defect emission around 450 nm. The Ce^{3+} emission intensity increases monotonically up to 900 K while the host emission decreases. Beyond 900 K, the emission spectrum is almost exclusively Ce^{3+} $4f5d$ emission which appears to begin quenching above 1000 K. The emission band shapes for both the Ce^{3+} and host emission in Ce:CSSO appear to be largely independent of temperature. Note that the measured spectra have a small peak near 532 nm; this is due to imperfectly rejected 532 or 266 nm scattered laser light.

Temperature-dependent emission spectra for the annealed Ce,Pr:CSSO phosphor are shown in Figure 5c. The co-doped spectrum contains contributions from the Pr^{3+} and Ce^{3+} $4f5d$ emission, as well as intrinsic host emission that was also observed in the Ce:CSSO sample. The host emission overlaps strongly with the Pr^{3+} emission band. As observed in the singly-doped phosphors, both the host-Pr^{3+} and Ce^{3+} emission bands exhibit an initial increase in signal intensity with temperature. For the host-Pr^{3+} emission band, the emission intensity is a maximum near 400 K, and significantly decreases with increasing temperature as a result of thermal quenching of the $4f5d$ emission at higher temperatures. For Ce^{3+}, the emission intensity increases continuously up to 800 K, before rapidly decreasing starting near 1000 K due to thermal quenching. There additionally appears to be a small decrease in emission intensity between 800 and 1000 K; it is not immediately clear what causes this decrease. As with the singly-doped Ce:CSSO sample, the Ce^{3+} and host-Pr^{3+} emission bands are separated with slight overlap around 450 nm. The emission bands are in good agreement with previous experimental studies [4, 5] and theory (based on the work of Dorenbos [23]). The co-doped spectra also contain a small peak near 532 nm resulting from imperfectly rejected laser light.

4.2. Emission lifetimes and relative signal

4.2.1. Emission lifetimes The results of the lifetime fits (the intensity-weighted average of the best-fit multi-exponential decay) are shown in Figure 6 for each ion and phosphor. Temperature uncertainty in the furnace is estimated to be no larger than 20 K, and lifetime uncertainty is estimated at 3 ns (equal to half of the laser pulse width). The Pr^{3+} lifetime in the singly-doped Pr:CSSO phosphor is around 35 ns at room temperature, and drops to ~16 ns at 600 K; the 50% quenching temperature (T_{50}) is approximately 600 K. This value is slightly lower than the value of >700 K reported by [5].

The Ce^{3+} lifetime in singly-doped Ce:CSSO is also shown in Figure 6 up to 1400 K. At room temperature the lifetime is approximately 60 ns and remains approximately constant up to 1000 K. It should be noted that the average lifetime actually increases slightly with increasing temperature up to a peak value of ~71 ns at 900 K. The increase in lifetime may be the result of host interference, as the intensity-weighted average lifetime is reported. However, this data shows that Ce^{3+} quenches in CSSO with a T_{50} of approximately 1230 K. To the authors' knowledge, this is the highest reported T_{50} for any garnet phosphor using fast allowed $4f5d$ emission.

The host emission lifetime results for Ce:CSSO are

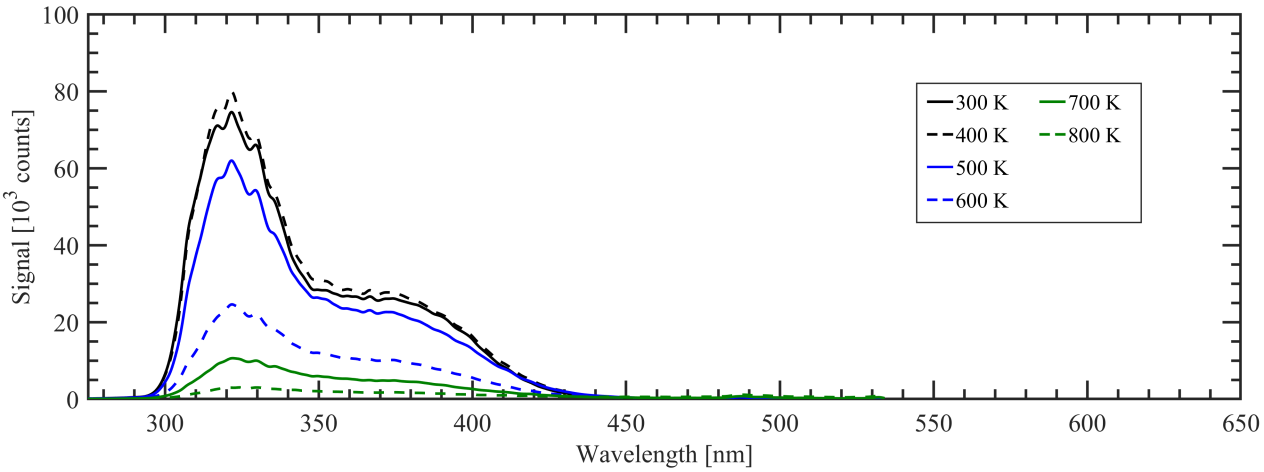

(a) Pr:CSSO

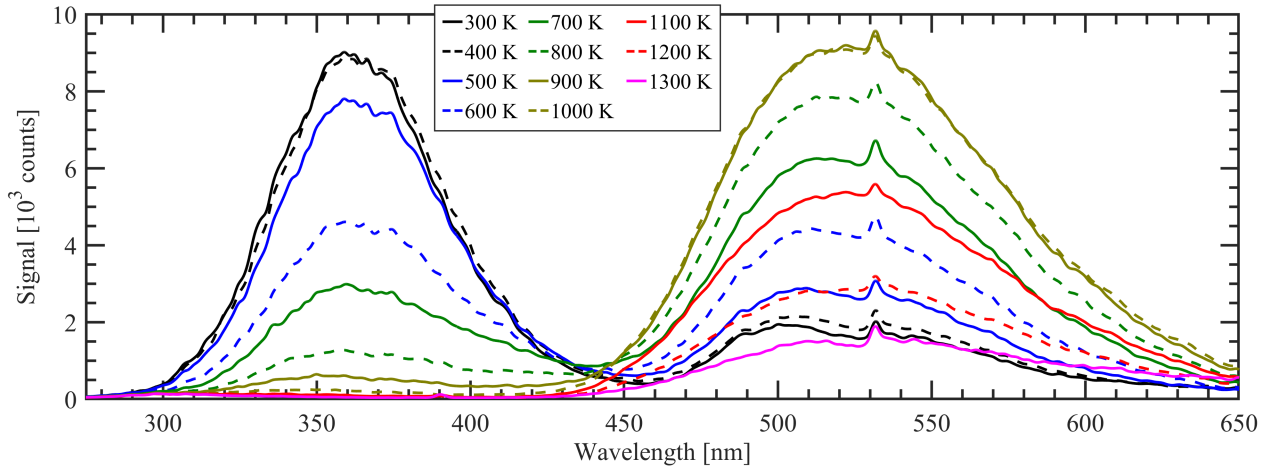

(b) Ce:CSSO

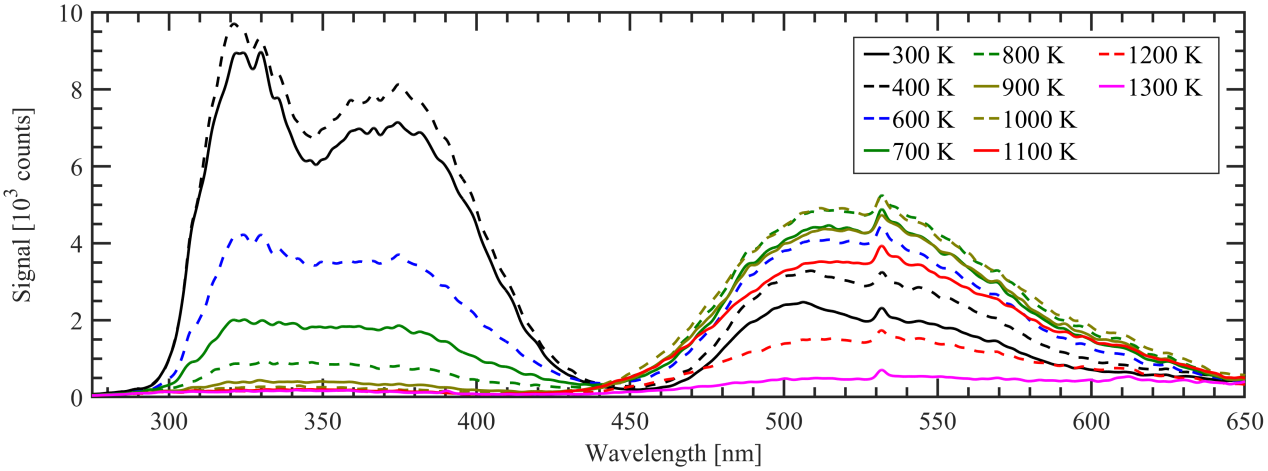

(c) Ce,Pr:CSSO

Figure 5: Measured emission spectra of each phosphor at 266-nm excitation: (a) Pr:CSSO, (b) Ce: CSSO, and (c) Ce,Pr:CSSO. Spectra are smoothed using a single-pass Gaussian filter with width of 2.5 nm. The small peak near 532 nm is due to imperfectly rejected 266 (2nd order) or 532 nm (1st order) laser light.

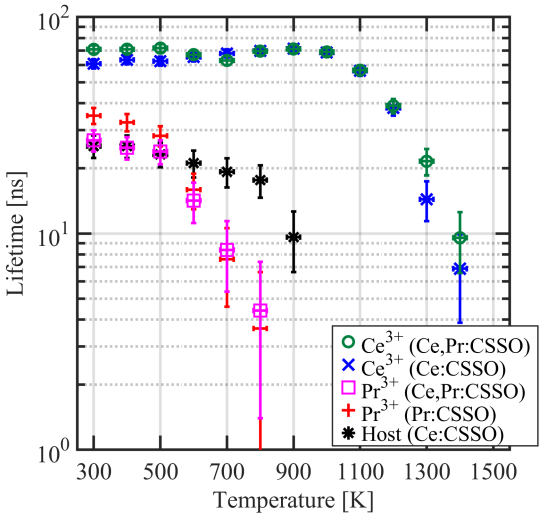

Figure 6: Measured lifetimes versus temperature for the Ce,Pr:CSSO, Ce:CSSO, and Pr:CSSO phosphors. Lifetimes are calculated as the intensity-weighted average of the best-fit multi-exponential decay. Note that Pr^{3+} band in the co-doped Ce,Pr:CSSO phosphor contains some portion of host emission in addition to the Pr^{3+} $4f5d$ emission. Error bars are estimated as 3 ns based on the width of the excitation laser pulse.

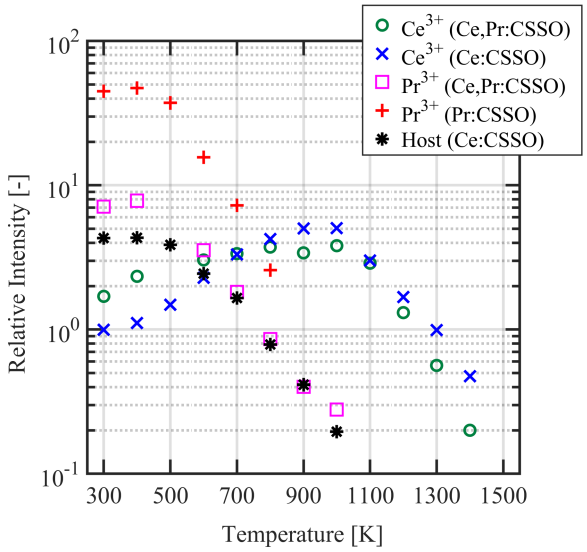

Figure 7: Measured emission intensity versus temperature for the Ce,Pr:CSSO, Ce:CSSO, and Pr:CSSO phosphors. "Host" refers to the host emission of the Ce:CSSO phosphor. Temperature dependence was calculated from integrated emission spectra, while integrated luminescence decay curves are used to determine the relative intensity of each series at 300 K.

shown in Figure 6, with a room temperature lifetime of 25 ns. Host emission appears to slowly begin quenching around 500 K with an abrupt decrease in the lifetime for temperatures greater than 800 K giving an effective T50 of approximately 850 K.

The lifetime of the host-Pr^{3+} emission band (containing both Pr^{3+} and host emission) for Ce,Pr:CSSO at room temperature is around 27 ns with a T_{50} near 600 K (similar to Pr^{3+} in the singly-doped Pr:CSSO phosphor). The room temperature lifetime is similar to that of the host emission observed in Ce:CSSO. The lifetime of the host-Pr^{3+} emission appears to be first dominated by the host, than at higher temperatures appears to more weighted towards the Pr^{3+} emission lifetime of the singly-doped phosphor. The observed behavior is impacted by the choice of collection band (295 nm to 425 nm) and if a different filter bandwidth was used different results would be obtained.

The Ce^{3+} emission band in the co-doped phosphor also appears to be influenced somewhat by host-Pr^{3+} emission. The Ce^{3+} band room temperature lifetime is increased to ~71 ns, slightly higher than the singly-doped result, but matches the singly-doped data well above 700 K after the Pr^{3+} and host emission have quenched considerably. The Ce^{3+} band of the co-doped Ce,Pr:CSSO phosphor has a T_{50} of ~1220 K, which matches well with the value from the singly-doped phosphor. Like the singly-doped phosphor this is the highest reported T_{50} for any garnet for $4f5d$ emission.

4.2.2. Relative signal The relative signals for each ion in both the co-doped and singly-doped CSSO phosphors were determined using the method described in Section 3.2. Results are shown versus temperature in Figure 7 normalized by the singly-doped Ce^{3+} signal at 300 K. Relative signal dependence on temperature follows a somewhat similar pattern as the lifetime for each ion and phosphor. However, for most cases, an increase in emission intensity is observed before the onset of quenching. The Ce^{3+} ion exhibits the largest increase in intensity, with the singly-doped phosphor showing a larger increase in Ce^{3+} emission than the co-doped phosphor.

Singly-doped Pr:CSSO has the brightest emission (before quenching), while Ce^{3+} in general has the lowest room-temperature signal. However, Ce^{3+} emission increases up to 950 K and does not quench significantly until 1200 K, making its signal intensity the strongest at temperatures > 700 K. In fact, for both the singly-doped and co-doped phosphors the Ce^{3+} signal is higher than its room temperature value until at least 1100 K. Therefore, is a viable option for temperature imaging above 1000 K as previously demonstrated for the singly-doped Ce:CSSO [2]. Interestingly, the co-doped and singly-doped

Ce^{3+} emission intensities are similar above 1000 K after the host and Pr^{3+} emissions have quenched significantly. At 900 K, the co-doped Ce^{3+} emission intensity appears to be lower than that at 800 and 1000 K; the cause is not immediately clear, but it may be related to interaction with the host.

Both the emission lifetime and relative signal results suggest potentially complex energy transfer behavior in the co-doped phosphor. However, overlap of host emission with emission from Pr^{3+}, and to a certain extent Ce^{3+}, makes it impossible to come to definitive conclusions from the data presented here. From a temperature diagnostic standpoint this does not impede our ability to design diagnostics and assess their performance, and relative signal results shown here are used later for diagnostic performance estimates.

The quenching results for all of the phosphors are summarized in Table 2, including estimated signal intensities and the 50% quenching temperature based on lifetime (T_{50}) and signal ($T_{50,S}$) for comparison. In general, the signal-based and lifetime-based 50% quenching temperatures are similar but not identical. In this case, $T_{50,S}$ and T_{50} are within 50 K except for the measurement of Ce:CSSO host emission.

4.3. Temperature sensitivity results

Using the temperature dependent relative signal results, the luminescence intensity ratio can be determined for each technique of interest. For Pr:CSSO the only technique considered is SRAPT. Since the Mie scattered signal is assumed to be constant (per particle) as a function of temperature, the SRAPT ratio for a given ion is determined by $R = S_i(300\text{ K})/S_i(T)$ where S_i is the relative signal for the band/ion of interest. For the co-doped phosphor, a SRAPT ratio can be determined for each ion, and a luminescence intensity ratio can be formed using the ratio of emission from the two ions. Here the collection band assumed for Pr^{3+} emission includes host emission for the co-doped phosphor. The co-doped ratio used here is given by

$$R_{\mathrm{Pr}^{3+}/\mathrm{Ce}^{3+}} = \frac{S_{\mathrm{Ce}^{3+}}(T)}{S_{\mathrm{Ce}^{3+}}(300\text{ K})}\frac{S_{\mathrm{Pr}^{3+}}(300\text{ K})}{S_{\mathrm{Pr}^{3+}}(T)}. \quad (6)$$

Finally, performance estimates for Ce:CSSO consider Ce^{3+} SRAPT, host SRAPT, and host-referenced APT. The host-referenced ratio is calculated in a fashion similar to the co-doped ratio for Ce,Pr:CSSO, where the Pr^{3+} emission band is replaced by the host emission.

Luminescence intensity ratios and temperature sensitivity for each APT technique for the singly-doped phosphors (Ce:CSSO and Pr:CSSO) are shown in Figure 8. The log of the Pr^{3+} and Ce^{3+} signal intensity data were fit using smoothing splines; the best-fit splines are used for performance prediction. The ratio results show the rapid increase in ratio once the temperature-dependent signal (*i.e.*, the signal in the denominator) begins to quench. The Ce^{3+} SRAPT ratio actually decreases with increasing temperature initially as a result of increasing signal for Ce^{3+} up to $\approx$ 1000 K. This causes some problems for temperature determination since there are two temperatures corresponding to the same ratio for temperatures below about 1200 K, and another piece of information is required to determine which is the correct temperature. The Pr^{3+} SRAPT ratio also shows an initial decrease and is double valued at low temperatures (below $\sim$450 K), but the increase in signal is very weak ($\sim$5%) and is not obvious on the scale used in Figure 8. Above 450 K the Pr^{3+} SRAPT ratio is monotonic. Both the host-referenced APT and host SRAPT ratios increase monotonically with temperature below 1000 K.

The rapid changes in SRAPT ratio result in high peak fractional temperature sensitivities shown in Figure 8b. Pr^{3+} SRAPT shows the largest sensitivity approaching 1%/K around 800 K. The Pr^{3+} SRAPT ratio additionally has zero temperature sensitivity around 350 K due to the initial increase in signal with temperature, but has greater than 0.5%/K sensitivity from about 500 to at least 800 K. The sensitivity of the Ce^{3+} SRAPT technique is also quite high at above 1000 K; however, due to the Ce^{3+} signal maximum at $\approx$1000 K, the Ce^{3+} SRAPT ratio has zero or close to zero temperature sensitivity from 850 to 1000 K. The host SRAPT technique with the Ce:CSSO phosphor has a similar peak temperature sensitivity near 0.75%/K as the Ce^{3+} SRAPT technique, but the peak occurs near 800 K. The host-referenced APT technique, which takes advantage of the simultaneous host quenching and Ce^{3+} signal increase from 400 to 900 K, has temperature sensitivity approaching 1%/K making it competitive with Pr^{3+} SRAPT.

The luminescence intensity ratio and sensitivity for the co-doped Ce,Pr:CSSO phosphor technique are shown in Figure 9. The ratio and sensitivity curves look similar to those for the singly-doped techniques with a few key differences. The Ce^{3+} SRAPT ratio in the co-doped phosphor increases faster with temperature than in the singly-doped Ce:CSSO phosphor, reaching a ratio of almost 10 at 1400 K (compared with a ratio near 2 at 1400 K in the singly-doped phosphor). This results in a higher temperature sensitivity of the Ce^{3+} SRAPT technique in the co-doped phosphor. In contrast, there is a reduction in sensitivity for the Pr^{3+} SRAPT band in the co-doped phosphor, possibly due to the additional host emission which quenches several hundred kelvins hotter

Table 2: Room temperature lifetime, estimated room temperature signal per particle (for 1.4 µm particle diameter), and 50% quenching temperatures (based on both lifetime and signal) for Ce^{3+} and Pr^{3+} in CSSO. Signal per particle is estimated from the relative emission intensity at room temperature, scaled by the signal per particle value for annealed Ce:CSSO (Ce^{3+}) from [2].

Phosphor (Band)	τ(300K) [ns]	S [photon/particle]	T_{50} [K]	$T_{50,S}$ [K]
Ce,Pr:CSSO (Ce^{3+})	70 ±3	1.7×10^4	1220 ±50	1170 ±50
Ce,Pr:CSSO (Pr^{3+})	27 ±3	7.1×10^4	620 ±50	590 ±50
Ce:CSSO (Ce^{3+})	60 ±3	1.0×10^4	1230 ±50	1220 ±50
Ce:CSSO (Host)	25 ±3	4.3×10^4	850 ±50	640 ±50
Pr:CSSO (Pr^{3+})	35 ±3	4.5×10^5	600 ±50	570 ±50

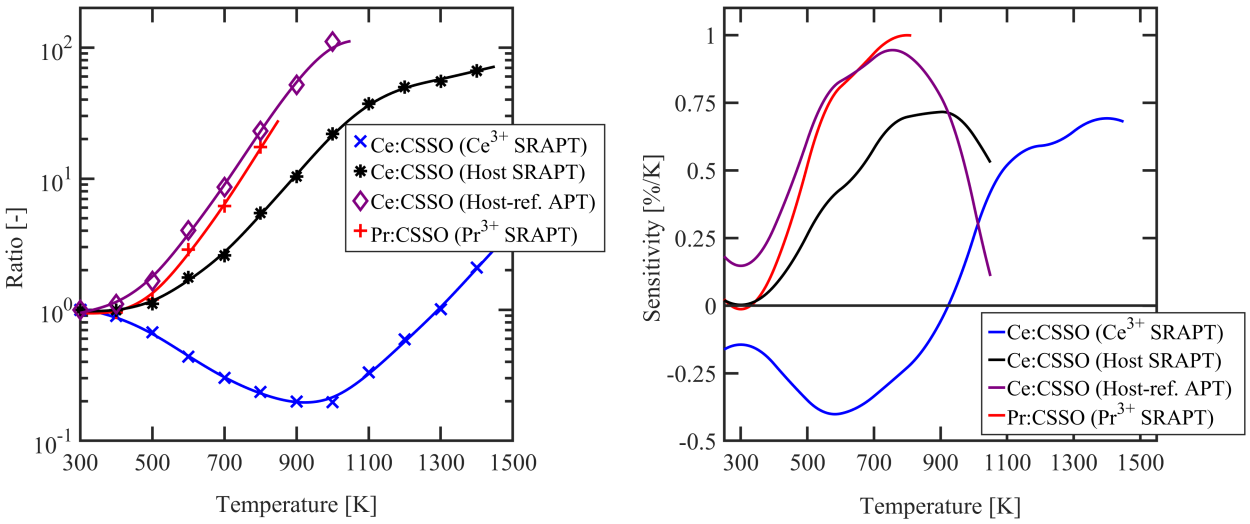

(a) Ratio (b) Sensitivity

Figure 8: Luminescence intensity ratio measurements and curve fits for each technique using the singly-doped Ce:CSSO and Pr:CSSO phosphors, and fractional temperature sensitivity calculated for each technique based on the ratio curve fits. "Host-ref. APT" refers to the host-referenced APT technique.

than Pr^{3+}. The co-doped ratio and sensitivity are very similar to those of the Ce,Pr:CSSO Pr^{3+} SRAPT technique, but the ratio increases more quickly due to the increase in Ce^{3+} intensity; this leads to a similar increase in diagnostic sensitivity. The co-doped ratio also has the advantage of slightly higher sensitivity at room temperature when compared with the Ce:CSSO host-reference APT technique, which is important for extending imaging down to room temperature. The co-doped Ce,Pr:CSSO phosphor overall has $\geq$ 0.25%/K fractional sensitivity from 300 K to 1400 K for at least one of the techniques.

4.4. APT diagnostic performance predictions

The quenching properties of the phosphors that were discussed in Section 4.2 suggest they may be suitable for temperature imaging in low-temperature combustion environments. Performance estimates for each phosphor and technique are made at a range of conditions in the aerosol phase that are intended to be relevant to low-temperature ignition in optically-accessible engines.

The temperature measurement precision index (standard deviation), s_T , is related to the temperature sensitivity and ratio precision index by Equation 3. One can relate the ratio precision index to the signal precision indices (s_{S_1} and s_{S_2}) through first order uncertainty propagation by

$$\left(\frac{s_R}{R}\right)^2 = \left(\frac{s_{S_1}}{S_1}\right)^2 + \left(\frac{s_{S_2}}{S_2}\right)^2 = \frac{F_1}{S_1} + \frac{F_2}{S_2} \tag{7}$$

where the right-hand side was rewritten assuming shot-noise limited detection, *i.e.*, $s_{S_i} = \sqrt{S_i}$ where S_i is the measured intensity, and F_i is the noise factor (used in the case where the detector for signal i is

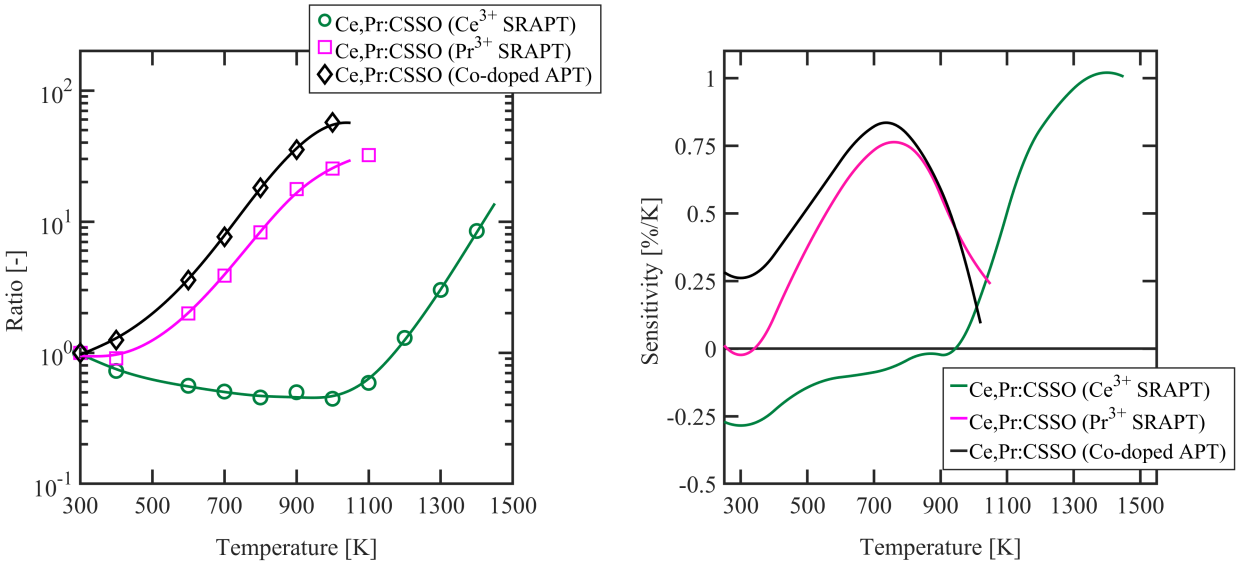

(a) Ratio (b) Sensitivity

Figure 9: Luminescence intensity ratio measurements and curve fits for each technique using the co-doped Ce,Pr:CSSO phosphor, and fractional temperature sensitivity calculated for each technique based on the ratio curve fits.

an intensified charge coupled device; ICCD). For a regular CCD or CMOS camera F=1. An additional noise term for SRAPT arises from the particle size distribution, where the particle diameter dependence of the measured ratio contributes noise due to the dispersion of particle diameters [8]. The SRAPT noise term is treated as a constant (*i.e.*, depends only on the number of imaged particles).

More generally, read noise could be included as well; however, ICCD cameras are often needed due to their fast gating capability to reject background signals in combustion environments and are typically designed and operated in such a way that read noise can be assumed negligible. Thus, these non-ideal effects will be ignored and a theoretical best-case performance will be presented. To include the effects of non-ideal amplifiers, the estimated temperature precision s_T can simply be multiplied by the $\sqrt{F_i}$ (F_i is typically between 1.6 and 4.2 for ICCD intensifiers at high gain [24]) to account for equipment limitations. For SRAPT, this should multiply the camera noise terms only, before adding the contribution from the particle size distribution.

To apply Equation 7 for performance estimates, a set of experimental parameters are required to estimate the room temperature signals (measured relative signal is used to infer signals at elevated temperatures). The required experimental parameters are given in Table 3. In particular, a target particle diameter of 1.0 µm is chosen, and per particle signal intensities (listed in Table 2) are scaled by particle volume (*i.e.*, $S_p \propto d^3$). Mathematically, the signal collected by camera i at room temperature is given by

$$S_i = S_{p,i} n V_c \eta_{QE} \eta_{opt} \frac{\Omega}{4\pi}, \tag{8}$$

where S_i is the captured signal in photons, $S_{p,i}$ is the room-temperature signal per particle value (scaled to the appropriate particle diameter d_p), and the remaining parameters are defined and specified in Table 3.

Two sets of optical properties are provided in Table 3; one for the visible band (Ce^{3+} emission) and one for the UV band (Pr^{3+} and host emission). The optical properties are for a relatively ideal system and thus represent an upper limit on diagnostic performance. The sensor is assumed to be hardware binned 4x4, such that the effective pixel length is ~0.5 mm in the object plane. For simplicity, the laser sheet thickness is chosen as 0.5 mm, making the binned collection volume approximately a cube. A seeding density of 1000 mm^{-3} is chosen as well; this corresponds to an added heat capacity of approximately 1% for an atmospheric flow at 1500 K, and thus has a negligible impact on the flow temperature particularly for the high air density expected in-cylinder. Since scattering intensity is typically several orders of magnitude larger than luminescence intensity, the contribution of noise in the scattering measurement is ignored in Equation 7 for SRAPT; instead the additional SRAPT noise term is included as $N_{PSD} = 0.1$ (such that the

Table 3: Assumed optical properties for performance prediction calculations. The bottom portion of the table lists derived properties.

Parameter	Visible	UV	Units
$f/\#$	1.4	2.0	-
Focal length, f	85	85	mm
Object distance, d_o	500	500	mm
Noise factor, F	1.0	1.0	-
Read noise, N_r	0	0	e^-
Optical eff., η_{opt}	0.9	0.8	-
Det. quantum eff., η_{QE}	0.5	0.3	-
Det. pixel size, L_p	27	27	µm
Hardware bin, b	4x4	4x4	-
Laser sheet width, w	0.5		mm
Seeding density, n	1000		mm^{-3}
Particle diameter, d_p	1.0		µm
SRAPT noise, N_{PSD}	0.1		-
Collection volume, V_c	0.127		mm^3
Collection fraction, $\Omega/4\pi$	4.3×10^{-4}		-
Magnification, M	0.20		-

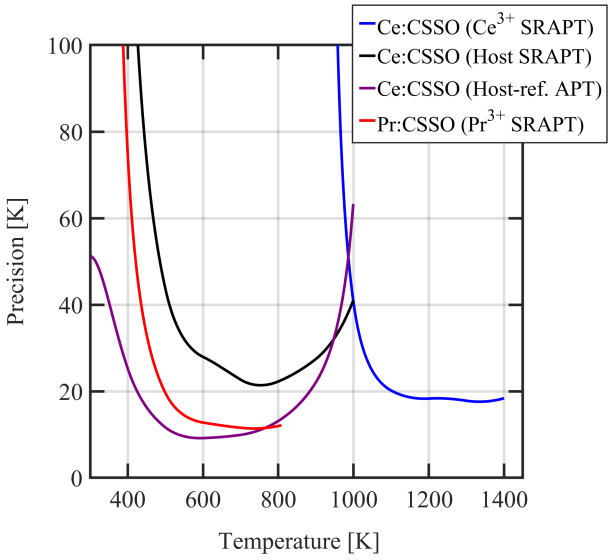

Figure 10: Estimated temperature precision for each technique using the singly-doped phosphors at constant seeding density and laser energy. "Host-ref. APT" refers to the host-referenced APT technique.

ratio measurement variance is increased by 0.1^2 or 0.01). Please refer to the Appendix for a complete mathematical description of the temperature precision calculation.

Estimated single-shot temperature precision using the assumed optical properties and approximate signal per particle values for the singly-doped phosphors are plotted in Figure 10. From the plot, the best temperature precision is achieved using the host-referenced APT technique with the Ce:CSSO phosphor between 500-800 K, where around 10 K single-shot precision is possible. The Pr^{3+} SRAPT technique with the Pr:CSSO phosphor is capable of similar precision in this temperature range. However, the host SRAPT technique with the Ce:CSSO phosphor provides the least precise measurement of any technique for the singly-doped phosphors. On a per particle basis, the Pr^{3+} emission band in the Pr:CSSO phosphor is significantly brighter than host emission, resulting in an improved temperature measurement. Above 1100 K, the Ce^{3+} SRAPT technique with the Ce:CSSO phosphor provides reasonable temperature precision (better than 20 K); this trend appears to continue to at least 1400 K. For the Ce^{3+} SRAPT technique, additional information is required to verify that the measured ratio corresponds to the high temperature range (> 900 K) as the ratio is double valued until almost 1300 K.

Temperature precision results for the co-doped Ce,Pr:CSSO phosphor are shown in Figure 11. As expected based on the temperature sensitivity results, co-doped APT using Ce,Pr:CSSO is capable of providing better single-shot temperature precision at low temperatures. Pr^{3+} SRAPT gives worse performance in the co-doped phosphor than for the singly-doped Pr:CSSO phosphor due to lower sensitivity. Ce^{3+} SRAPT was only considered in the high temperature region (T > 1000 K) for the calculations shown here. The results indicate that Ce^{3+} SRAPT using the co-doped phosphor is slightly less precise at temperatures near and slightly greater than 1000 K, but shows better precision for temperatures > about 1100 K due to higher sensitivity. As with the singly-doped Ce^{3+} SRAPT technique, it is important to note that from 1000 K to approximately 1200 K additional information is required to verify that the ratio measured corresponds to this temperature range since the Ce^{3+} SRAPT ratio is double valued up to 1200 K.

Based on the estimated precisions (using a metric of 40-K single-shot precision), singly-doped Pr:CSSO appears feasible for single-shot measurements from approximately 425 K to at least 800 K. Singly-doped Ce:CSSO using a combination of host-reference APT, host SRAPT, and Ce^{3+} SRAPT appears feasible for single-shot measurements from 350 K to at least 1400 K, although precision will be marginal in the 950 to 1050 K range. The co-doped Ce,Pr:CSSO phosphor extends the low end of the temperature measurement range, and single-shot measurements appear feasible from 300 K to 925 K and from 1030 K to at least 1400 K. It should be noted that with the Ce:CSSO

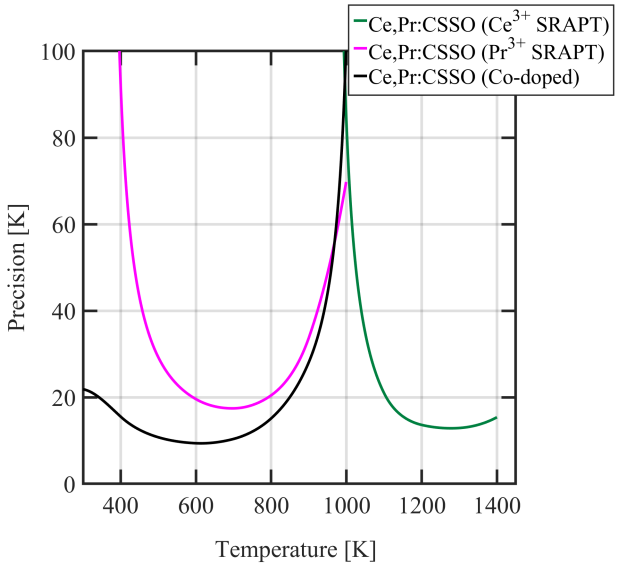

Figure 11: Estimated temperature precision for each technique using the co-doped Ce,Pr:CSSO phosphor at constant seeding density and laser energy.

and Ce,Pr:CSSO phosphors, the three measurements mentioned can be made simultaneously (Ce^{3+} SRAPT, host SRAPT, and host-referenced APT for Ce:CSSO; and Ce^{3+} SRAPT, Pr^{3+} SRAPT, and co-doped APT for Ce,Pr:CSSO), allowing the entire temperature range stated to be covered in a single experiment (please refer to [2, 25] for a detailed discussion relating to the combination of APT techniques). Additionally, PIV can be performed simultaneously using the Mie scattering signal acquired for SRAPT measurements.

The Ce^{3+} SRAPT performance predictions for both Ce:CSSO and Ce,Pr:CSSO suggest a feasible temperature range for APT that extends to at least 1400 K. However, in both cases there is a gap from approximately 950-1050 K (resulting from the double-valued ratio function) where temperature precision is only marginal. Overall, these results indicate that the Ce:CSSO and Ce,Pr:CSSO phosphors are promising for imaging over broad temperature ranges and provide capability to extend single-shot APT temperature imaging to at least 1400 K. Temperature imaging with the singly-doped Ce:CSSO phosphor has already been demonstrated up to 1400 K [2].

5. Conclusions

Characterization results for Pr:CSSO, Ce:CSSO, and Ce,Pr:CSSO demonstrate that these phosphors are promising candidates for APT temperature imaging. The phosphors were characterized in a tube furnace up to 1400 K, and comparisons were made between the co-doped phosphor and its' singly-doped counterparts. Of the singly-doped phosphors, Pr:CSSO has the highest temperature sensitivity of ∼1%/K at 800 K, while the Ce:CSSO Ce^{3+} SRAPT technique has a peak sensitivity of near 0.7%/K at 1400 K. The co-doped phosphor has similar temperature sensitivity, with >0.25%/K sensitivity throughout the temperature range from 300 to 1400 K, and a peak temperature sensitivity near 1%/K above 1200 K using Ce^{3+} SRAPT. The emission wavelengths of the two ions in the co-doped phosphor are spectrally separated such that the phosphor can be used for the co-doped APT approach. However, the introduction of Ce^{3+} into CSSO appears to result in a significant amount of host emission and interaction between the host and ions. These results provide the first high-temperature characterization of the Ce,Pr:CSSO phosphor, and represent the first reported measurements of the quenching temperatures of Ce^{3+} and Pr^{3+} co-doped in CSSO. Estimates of emission intensity and diagnostic performance suggest that the Ce:CSSO and Ce,Pr:CSSO phosphors may be capable of precise APT imaging at temperatures from 300 K up to at least 1400 K using a combination of APT approaches, while the singly-doped Pr:CSSO phosphor may be capable of precise temperature imaging from 425 to over 800 K.

Acknowledgements

Research was sponsored by the Army Research Office and was accomplished under Grant Number W911NF-19-1-0238. The views and conclusions contained in this document are those of the authors and should not be interpreted as representing the official policies, either expressed or implied, of the Army Research Office or the U.S. Government. The U.S. Government is authorized to reproduce and distribute reprints for Government purposes notwithstanding any copyright notation herein.

References

[1] Abram C, Fond B and Beyrau F 2018 *Progress in energy and combustion science* **64** 93–156
[2] Herzog J M, Witkowski D and Rothamer D A 2020 *Proceedings of the Combustion Institute*
[3] Yin Z, Fond B, Eckel G, Abram C, Meier W, Boxx I and Beyrau F 2017 *Combustion and Flame* **184** 249–251
[4] Sharma S K, Lin Y C, Carrasco I, Tingberg T, Bettinelli M and Karlsson M 2018 *Journal of Materials Chemistry C* **6** 8923–8933
[5] Ivanovskikh K, Meijerink A, Piccinelli F, Speghini A, Zinin E, Ronda C and Bettinelli M 2010 *Journal of Luminescence* **130** 893–901
[6] Witkowski D and Rothamer D A 2019 *Proceedings of the Combustion Institute* **37** 1393–1400
[7] Nikolić M G, Antić Ž, Ćulubrk S, Nedeljković J M and Dramićanin M D 2014 *Sensors and Actuators B: Chemical* **201** 46–50

[8] Witkowski D and Rothamer D A 2019 *Measurement Science and Technology* **30** 044003

[9] Yamamoto H 2007 Luminescence of a localized center *Phosphor Handbook* ed Yen W M, Shionoya S and Yamamoto H (Boca Raton, FL: CRC Press/Taylor and Francis) book section 2.3, pp 35–47 2nd ed

[10] Amachraa M, Wang Z, Chen C, Hariyani S, Tang H, Brgoch J and Ong S P 2020 *Chemistry of Materials* **32** 6256–6265

[11] Witkowski D and Rothamer D A 2017 *Journal of Luminescence* **192** 1250–1263

[12] Dorenbos P 2020 *Journal of Luminescence* 117164

[13] Lin Y C, Bettinelli M and Karlsson M 2019 *Chemistry of Materials* **31** 3851–3862

[14] Dorenbos P 2005 *Journal of Physics: Condensed Matter* **17** 8103

[15] Justel T 2019 (accessed October 2, 2019) *Phosphor Information and Spectra Access (PISA)* URL `fh-muenster.de/ciw/personal/professoren/juestel/pisa.php`

[16] Halvorson H R 1992 Padé-laplace algorithm for sums of exponentials: Selecting appropriate exponential model and initial estimates for exponential fitting *Methods in enzymology* vol 210 (Elsevier) pp 54–67

[17] Akaike H 1974 *IEEE transactions on automatic control* **19** 716–723

[18] Pereyra V and Scherer G 2010 *Exponential data fitting* (Bentham Science Publishers) pp 1–26

[19] Brübach J, Janicka J and Dreizler A 2009 *Optics and Lasers in Engineering* **47** 75–79

[20] Lakowicz J R 2013 *Principles of fluorescence spectroscopy* (Springer science & business media)

[21] Nagasawa D, Mondrik N, Marshall J, DePoy D, Schmidt L, Hill B, Turner L and Rheault J 2016 Throughput of commercial photographic camera lenses for use in astronomical systems *Ground-based and Airborne Instrumentation for Astronomy VI* vol 9908 (International Society for Optics and Photonics) p 99085C

[22] Fond B, Abram C, Pougin M and Beyrau F 2019 *Optical Materials* **89** 615–622

[23] Dorenbos P 2019 *Journal of Luminescence* **214** 116536

[24] Moran S E, Ulich B L, Elkins W P, Strittmatter R J and DeWeert M J 1997 Intensified CCD (ICCD) dynamic range and noise performance *Ultrahigh-and High-Speed Photography and Image-based Motion Measurement* vol 3173 (International Society for Optics and Photonics) pp 430–457

[25] Herzog J M, Witkowski D and Rothamer D A *manuscript submitted for publication*

Appendix A. Temperature Precision Calculation

All of the thermometry techniques discussed are ratiometric, intensity-based methods, where a ratio R is formed between two temperature-dependent signals (S_1 and S_2) such that

$$R = \frac{S_2}{S_1}, \tag{A.1}$$

and R is a function of only temperature. The temperature precision can be estimated from a first-order uncertainty propagation via

$$s_T \approx \left|\frac{dT}{dR}\right| s_R = \frac{s_R}{R}\frac{1}{\xi_T} \tag{A.2}$$

where

$$\xi_T = \frac{1}{R}\frac{\partial R}{\partial T} \tag{A.3}$$

is the temperature sensitivity of the technique. Performing a similar uncertainty propagation on Equation A.1, the ratio precision can be written as

$$\left(\frac{s_R}{R}\right)^2 \approx \left(\frac{s_{S_2}}{S_2}\right)^2 + \left(\frac{s_{S_1}}{S_1}\right)^2 + N_{PSD}, \tag{A.4}$$

where the SRAPT noise term is included to account for any effects resulting from the particle size distribution. The noise on an ICCD camera can be estimated as

$$s_{S_i}^2 \approx N_{r,i} + F_i S_i, \tag{A.5}$$

where S_i is the measured signal in photons (representing the shot-noise contribution), F_i is the noise factor, and $N_{r,i}$ is the read noise. Assuming the camera is shot-noise limited, $N_{r,i} \approx 0$ and

$$\left(\frac{s_R}{R}\right)^2 \approx \frac{F_2}{S_2} + \frac{F_1}{S_1} + N_{PSD}^2, \tag{A.6}$$

which is identical to Equation 7, but including the SRAPT noise term. Finally, combining Equations A.2 and A.6, the temperature precision can be calculated as

$$s_T = \frac{\sqrt{\frac{F_1}{S_1} + \frac{F_2}{S_2} + N_{PSD}^2}}{R\xi_T}. \tag{A.7}$$

For SRAPT techniques, the shot-noise in the scattered laser light is negligible because S_2 is very large. Similarly, in co-doped and host-referred techniques the PSD noise is zero because the signals S_1 and S_2 have the same diameter dependence.

For performance prediction, it is necessary to estimate the number of photons collected on each detector. The number of photons collected on a detector is equal to the total number of photons emitted inside the detector's collection volume, multiplied by the collection efficiency. The collection efficiency is given by

$$\eta = \eta_{QE}\eta_{opt}\frac{\Omega}{4\pi}, \tag{A.8}$$

where η_{QE} is the detector quantum efficiency, η_{opt} is the optical transmission efficiency (due to the camera lens and filters), and Ω is the collection solid-angle of the lens. The number of photons emitted inside the collection volume is given by

$$S_{0,i} = S_{p,i}(d_p) n V_c, \tag{A.9}$$

where $S_{p,i}(d_p)$ is the phosphor signal per particle, n is the phosphor seeding density, and V_c is the sensor's collection volume,

$$V_c = \left(\frac{bL_p}{M}\right)^2 w. \tag{A.10}$$

The phosphor signal per particle was reported in Table 2 for the 1.4 µm diameter particle; this value is scaled to the assumed 1.0 µm diameter according to

$$S_{p,i}(d_p) = S_{p,i}(d_{p,0})\left(\frac{d_p}{d_{p,0}}\right)^3 \tag{A.11}$$

where $d_{p,0}$ is the original 1.4 µm particle diameter. Finally, combining Equations A.8, A.9, and A.11, the signal collected on a sensor in photons is given by

$$S_i = S_{p,i}(d_{p,0})\left(\frac{d_p}{d_{p,0}}\right)^3 nV_c\eta_{QE}\eta_{opt}\frac{\Omega}{4\pi}. \tag{A.12}$$